Dalton Transactions

Accepted Manuscript

ROYAL SOCIETY OF CHEMISTRY

www.rsc.org/dalton

Enhancement of thermoelectric properties by Na doping in Te-free p-type $AgSbSe_2$

Songting Cai[⊥], Zihang Liu[⊥], Jianyong Sun, Rui Li, Weidong Fei and Jiehe Sui*

School of Materials Science and Engineering, P.O. Box 405, Harbin Institute of Technology, Harbin, 150001, China

[⊥]equal contributors.

Corresponding author. E-mail address: suijiehe@hit.edu.cn

Abstract

$AgSbSe_2$ possesses extremely low thermal conductivity and high Seebeck coefficient, but the low electronic conductivity leads to low ZT value. In this paper, Na is used to substitute Sb to improve the electronic conductivity. The results show that Na doping not only improves the power factor caused by the enhanced carrier concentration, but also decreases the thermal conductivity due to point defects, nanoscale stacking faults and Na-rich precipitate. Consequently, a high ZT value of 0.92 is achieved in the $AgSb_{0.99}Na_{0.01}Se_2$ sample.

1. Introduction

Thermoelectric materials and devices can directly and reversibly convert heat energy into electrical energy and will play a significant role in the application of power generation and cooling.[1-3] The conversion efficiency of thermoelectric devices is determined by the dimensionless figure of merit $ZT = (S^2\sigma/k)\ T$, where S, σ, κ, and T

are the Seebeck coefficient, electrical conductivity, thermal conductivity, and absolute temperature, respectively. Generally, the thermal conductivity is the sum of the lattice and electronic thermal conductivity ($\kappa_{total} = \kappa_{latt} + \kappa_{ele}$). Therefore, improving power factor ($S^2\sigma$) and decreasing lattice thermal conductivity are considered effective method in improving thermoelectric performance. In the past decades, much effort had been made to improve power factor ($S^2\sigma$) by band engineering,[4-6] quantum confinement,[7] and lattice thermal conductivity reduction via point defects and nanostructuring,[8-10] consequently leading to improve ZT value of thermoelectric mateials, such as Bi_2Te_3-based,[11-13] PbTe-based,[5,6,9] GeSi,[14,15] etc.

Thus far, most of the state-of-the-art thermoelectric materials, such as Bi_2Te_3,[11-13] PbTe,[5, 6, 9] $AgSbTe_2$,[16, 17] are composed of Te, which is a rare and toxic element on earth.[18] Thus, it is imperative to develop an alternative Te-free thermoelectric material. Currently, Te-free compounds including $CoSb_3$,[19, 20] Half-heusler,[8, 21] PbSe,[22] PbS,[23] Mg_2Si,[24,25] In_4Se_3[26] have been developed and drawn increasingly scientific attentions. Exploring new type high performance Te-free thermoelectric materials is still a hot issue.

Te-free $AgSbSe_2$, a member of the cubic bulk I–V–VI_2 compounds family (where I = Cu, Ag, Au or alkali metal; V = As, Sb, Bi; and VI = Se, Te), processes low thermal conductivity and high Seebeck coefficient, displaying a potential to have high performance thermoelectric materials. However, the low conductivity results in the modest ZT value. Therefore, the purpose of study is to improve the electrical transport properties of $AgSbSe_2$, further improving the ZT value. Recently, a small amount of

metal ion (Pb^{2+}, Cd^{2+}, Zn^{2+} or Bi^{3+}) doping in single phase $AgSbSe_2$ enhances the electrical transport by increasing carrier concentration, consequently leading to a ZT value above unity.[27-28] Na has been considered as an ideal hole dopant in PbX (X=S, Se and Te) based thermoelectric materials.[23, 30] To our knowledge, thermoelectric properties of $AgSbSe_2$ doping with sodium have not been investigated previously. Herein, effect of Na concentration on the microstructure and thermoelectric properties of $AgSb_{1-x}Na_xSe_2$ (x=0, 0.5%, 1%, 2%) is investigated. Our investigation on the thermoelectric properties of $AgSb_{1-x}Na_xSe_2$ proves that a very small amount of Na, $AgSb_{0.99}Na_{0.01}Se_2$, has resulted in a lower thermal conductivity and higher power factor, leading to a high ZT value of 0.92.

2. Experimental section

According to the chemical composition $AgNa_xSb_{1-x}Se_2$（x=0、0.005、0.01、0.02）, appropriate amount of raw materials, Ag (4N), Sb (4N), Se (5N) and Na_2Se (3N), which are all purchased from Alfa Aesar, were mixed uniformly in the glove box, and then cold pressed into pellets cylinder. The pellets were sealed with silica tubes, melted for 8h at 1023K, and then quenched to room temperature. The obtained products were crushed into powders by hand, and then densified by hot press sintering at 723 K for 2.5 h under the axial compressive stress of 90 MPa.

All the powder diffraction patterns (XRD) were obtained using a PANa-lytical multipurpose diffractometer with an X'celerator detector (PANalytical X'Pert Pro). Scanning electron microscopy (SEM) and transmission electron microscope (TEM)

studies were performed using a HELIOS NanoLab 600i, FEI and Tecnai G^2 F30, FEI, respectively. Samples used for TEM observations were similar with our previous reports [31]. Seebeck coefficient and the electrical conductivity are simultaneously measured using ZEM-3 (ULVAC-RIKO) for all samples with the dimensions of ~2.5×2.5×11 mm^3. The thermal conductivity was calculated from $\kappa=DC_p\rho$. The thermal diffusivity (D) is measured by Netzsch LFA427 (NETZSCH, LFA457, Germany) using a polished disk with a 12.7 mm diameter, and thickness1.5 mm. The specific heat capacity (C_p) is calculated by using the Dulong-Petit law, namely Cp= 3R/M, where R is the gas constant and M is molar mass. And the obtained value (C_p= 0.2565) was close to the measured result [27]. The density (ρ) was determined by the Archimedes method. Densities of the samples are ~96 % of the theoretical density. The Hall coefficients (R_H) were measured at room temperature using a Hall Effect measurement system (SWIN, Hall8800, Taiwan) with a magnetic field of 0.5 T applied.

3. Results and Discussion

Figure 1a shows powder XRD patterns of $AgNa_xSb_{1-x}Se_2$（x=0, 0.005, 0.01, 0.02） samples from 20 ° to 60°. All the Bragg peaks show a perfect match to $AgSbSe_2$ (PDF#12-0379) with space group $Fm\bar{3}m$ without the impurity phase within the detection limit of powder XRD. As illustrated in Figure 1b, the main diffraction peak of $AgNa_xSb_{1-x}Se_2$ samples abruptly shifts to lower diffraction angles when Na content is increased to 0.5%, and then has no obvious change with further increasing the Na

content from 1% to 2%. Obviously, for $AgNa_{0.01}Sb_{0.99}Se_2$ and $AgNa_{0.02}Sb_{0.98}Se_2$ samples, the main diffraction peaks become wider compared with 0.5% Na doping sample shown in Figure 1b, which may be resulted from the appearance of the precipitates (discussed later). As shown in Figure 1c, the lattice parameters calculated from the power XRD data remarkably increase first and then keep saturated. The increased lattice parameter can be attributed to the difference of ionic radius between Na^+ (~0.97 Å) and Sb^{3+} (~0.92 Å). The saturated lattice parameter indicates the 0.5% Na or less is the solubility limit. Carrier concentration listed in Table 1 is also markedly increase first when Na content is 0.5%, and then increase slowly when the Na content is further increased, which can be indirectly confirm the solubility limit is 0.5% or less.

Figure 2 shows the morphology of the fresh fractured surface and elemental distribution of sample $AgNa_{0.01}Sb_{0.99}Se_2$. From Figure 2a, the grain size of $AgNa_{0.01}Sb_{0.99}Se_2$ range from 20 μm to 40 μm. Furthermore, random microholes and white microprecipities can be observed in the matrix and along the grain boundary as shown in Figure 2b. It is the microholes and precipitates that will have an effect on the electrical transport properties and thermal conductivity, which will be discussed later. Apart from the precipitate, the elements are homogeneously distributed throughout the sample shown in Figure 2c-f. It can be concluded that the precipitate is Na-rich second phase from the color contrast of Na element distribution shown in Figure 2f. The appearance of microprecipitates is mainly caused by the wide gap of electronegativity and atomic mass between Na and Sb elements, which results in the

low solid solubility of Na formed in the $AgSbSe_2$ solid solution. However, the specific composition and structure of Na-rich microprecipitate is still an open issue that needs to be further addressed.

In order to further investigate the microstructures of the $AgSbSe_2$ system, the hot pressed samples of pristine $AgSbSe_2$ and $AgNa_{0.01}Sb_{0.99}Se_2$ were examined by high resolution transmission electron microscopy (HRTEM). Figure 3a displays the high-magnification TEM image of pristine $AgSbSe_2$ as well as the fast Fourier transform (FFT) pattern, which can be indexed into $AgSbSe_2$ with space group $Fm\bar{3}m$ along the $[1\bar{1}1]$C zone axis. In addition, after careful and plentiful observations, crystal defects within the field of version are not found. However, large amount of stacking faults can be clearly seen in the sample of $AgNa_{0.01}Sb_{0.99}Se_2$ marked with red rectangle in the Figure 3b. The fast Fourier transform (FFT) pattern also confirms the existence of stacking faults, which may be resulted from the decrease of stacking fault energy generated by the supersaturation of Na formed in the $AgSbSe_2$ solid solution.[32]

Figure 4 presents the temperature dependence of thermoelectric properties for $AgNa_xSb_{1-x}Se_2$（x=0, 0.005, 0.01, 0.02）samples. The temperature-dependent electrical conductivity was plotted in Figure 4a. With increasing the Na content, the electrical conductivity increases first and then decreases at the measured temperature range from room temperature to 673K, consistent with the previous results.[28, 29] Taking the electrical conductivity of room temperature as an example, electrical conductivity significantly increases from 26 S cm^{-1} for the pristine $AgSbSe_2$ to 60 S cm^{-1} for the $AgNa_{0.01}Sb_{0.99}Se_2$ sample, and then decrease to 46 S cm^{-1} for the $AgNa_{0.02}Sb_{0.98}Se_2$

sample. Table 1 lists the measured room temperature carrier concentration and mobility of $AgNa_xSb_{1-x}Se_2$ samples. The carrier concentration of $AgNa_xSb_{1-x}Se_2$ increases markedly from 7.7×10^{18} cm^{-3} for pristine $AgSbSe_2$ to 3.1×10^{19} cm^{-3} for $AgNa_{0.005}Sb_{0.995}Se_2$, and then increases to 4.2×10^{19} cm^{-3} For the improved carrier concentration of $AgNa_{0.005}Sb_{0.995}Se_2$, it can be explained that each Na^+ atom substituting for Sb^{3+} atom will generate two holes from simple valence electron counting. When the Na content is above 0.5%, the precipitates are occurred, leading to that the factors influencing the carrier concentration become complicated. Therefore, the further increased hole carrier concentration may be ascribed to appearance of the Na-rich precipitate. The carrier mobility is decreased from 29.1 $cm^2 V^{-1} s^{-1}$ to 6.6 $cm^2 V^{-1} s^{-1}$ with increasing the Na content listed in Table 1, which can be ascribed to the point defect scattering between the Na and Sb and the appearance of the precipitates. Therefore, the increased electrical conductivity can be mainly attributed to the increased carrier concentration when the Na content is increased from 0 to 1%, while the decreased electrical conductivity of $AgNa_{0.02}Sb_{0.98}Se_2$ can be mainly ascribed to the decreased carrier mobility.

Figure 5b shows the temperature dependent Seebeck coefficient of $AgNa_xSb_{1-x}Se_2$. The positive Seebeck coefficient values indicate that all the samples are p-type semiconductors. The overall Seebeck coefficient of Na doped $AgSbSe_2$ is much lower than that of $AgSbSe_2$, which can be ascribed to the increased the carrier concentration shown in Table 1. With increasing the Na content, the Seebeck coefficient is decreased first and then increased, displaying an opposite trend with the

electrical conductivity. Therefore, the change of Seebeck coefficient, similar to electrical conductivity, is also related to the carrier concentration and mobility.

Power factor ($P=S^2\sigma$) calculated from the measured electrical conductivity and Seebeck coefficient for the $AgNa_xSb_{1-x}Se_2$ samples as shown in Figure 5c. The Na doped samples have higher power factors than $AgSbSe_2$, especially for $AgNa_{0.01}Sb_{0.99}Se_2$ sample with power factor of 5.7 μW cm^{-1} K^{-2} at 573 K, which is comparable to Pb or Cd doped $AgSbSe_2$.[27, 29]

Figure 5d reveals the total thermal conductivity, κ_{total}, for $AgNa_xSb_{1-x}Se_2$ samples. Plainly, the κ_{total} of pristine $AgSbSe_2$ is extremely low, caused by the lone pair of Sb element and highly disordered Ag/Sb lattice, which is much lower than that of high performance thermoelectric material.[9, 11, 17] Generally, the κ_{total} consists of two parts, including the lattice thermal conductivity (κ_{lat}), and the electronic thermal conductivity (κ_{ele}). Therefore, the κ_{lat} can be obtained by directly subtracting κ_{ele} from κ_{total}, in which the κ_{ele} is calculated through the Wiedemann-Franz relationship, $\kappa_{ele} = L \sigma T$, where L is the Lorenz number. In this work, the Lorenz number is obtained by fitting the respective Seebeck coefficient values with an estimate of the reduced chemical potential, rather than using a constant value.[23] Figure 5e shows the κ_{lat} for $AgNa_xSb_{1-x}Se_2$ samples. For the Na doped samples (x=0.005 and 0.01), the total thermal conductivity is lower than that of pristine $AgSbSe_2$ sample. Even though the electrical conductivity of the Na doped samples is higher than that of the $AgSbSe_2$ sample (Figure 5a), meaning the electronic thermal conductivity of the Na doped samples is higher than that of $AgSbSe_2$. However, the total thermal conductivity of the

Na doped samples is rather lower, indicating the fact that Na is indeed effective on reducing the lattice thermal conductivity. It can be explained that the presence of point defects, nanoscale stacking faults and microprecipitates as a panoscopic approach result in the scattering of heat-carrying phonons across multiple length scales.[9] Firstly, point defects caused by mass fluctuation and strain fluctuations between Na atom and Sb atom and nanoscale stacking faults will strengthen scattering phonons with short and medium mean free paths,[34] consequently leading to decrease the thermal conductivity without deteriorating the electrical conductivity. Besides, mesoscale grain boundaries of precipitates continue to scatter phonons with longer mean free paths. It is obvious that owing to the multiscale hierarchical architecture, 1% Na doping sample show much lower κ_{lat}, which decrease nearly 33% compared with the pristine $AgSbSe_2$ sample at room temperature.

Figure 5f shows the *ZT* values of the $AgNa_xSb_{1-x}Se_2$ samples. Compared with the pristine $AgSbSe_2$ sample, the decreased thermal conductivity and the improved power factor lead to higher peak and average *ZT* values in the Na doped samples. We achieved *ZT*s of 0.92 at 673K in sample $AgNa_{0.01}Sb_{0.99}Se_2$, comparable to the *ZT*s of Pb, Cd and Bi doped $AgSbSe_2$ sample within the experimental errors of *ZTs* of about 10-12%.

4. Conclusion

In summary, the $AgNa_xSb_{1-x}Se_2$（x=0、0.005、0.01、0.02）samples are prepared by using melting and hot pressing methods. Upon Na doping, the electrical conductivity

is significantly increased due to the increased hole carrier concentration via Na^{+} atom substituting for Sb^{3+} atom. Meanwhile, the total thermal conductivity is simultaneously depressed, which can be ascribed to the scattering of heat-carrying phonons across multiple length scales by the presence of point defects, nanoscale stacking faults and microprecipitates. As a result, a high ZT = 0.92 is obtained for the $AgNa_{0.01}Sb_{0.99}Se_2$ sample at 673 K. Further enhancing thermoelectric performance can be achieved by co-doping to increase electrical transport properties or making grain refining to decrease the thermal conductivity.

Acknowledgements

This work was supported by the National Natural Science Foundation of China (No.51471061 and 51271069). This contribution was also supported by the Program for New Century Excellent Talents in University of Ministry of Education of China (NCET-12-0160).

References

[1] G.J. Snyder and E.S. Toberer, Nat. Mater., 2008, 7, 105.

[2] M. Zebarjadi, K. Esfarjani, M. S. Dresselhaus, Z. F. Ren, G. Chen, Energy Environ Sci., 2012, 5, 5147.

[3] J. R. Sootsman, D. Y. Chung and M. G. Kanatzidis, Angew.Chem. Int. Ed., 2009, 48, 8616.

[4] Y. Z. Pei, H Wang, and G. J. Snyder, Adv. Mater., 2012, 24, 6125.

[5] J. P. Heremans, V. Jovovic, E. S. Toberer, A. Saramat, K. Kurosaki, A. Charoenphakdee, S.Yamanaka and G. J. Snyder, Science., 2008, 321, 554.

[6] Y. Z. Pei, X. Y. Shi, A. LaLonde, H. Wang, L. D. Chen and G. J. Snyder, Nature., 2011, 473, 66.

[7] L. D. Hicks, T. C. Harman, X. Sun and M. S. Dresselhaus, Phys. Rev. B., 1996, 53, 10493.

[8] X. Yan, G. Joshi, W. S. Liu, Y. C. Lan, H. Wang, S. Lee, J. W. Simonson, S. J. Poon, T. M. Tritt, G. Chen, and Z. F. Ren, Nano Lett., 2011, 11, 556.

[9] K. Biswas, J. He, I. D. Blum, C. I. Wu, T. P. Hogan, D. N. Seidman, V. P. Dravid and M. G.Kanatzidis, Nature., 2012, 489, 414.

[10] L. D. Zhao, J. Q. He, S. Q. Hao, C. I. Wu, T. P. Hogan, C. Wolverton, V. P. Dravid and M. G.Kanatzidis, J. Am. Chem. Soc., 2012, 134, 16327.

[11] B. Poudel, Q. Hao, Y. Ma, Y. C. Lan, A. Minnich, B. Yu, X. A. Yan, D. Z. Wang, A. Muto, D. Vashaee, X. Y. Chen, J. M. Liu, M. S. Dresselhaus, G. Chen and Z. F. Ren, Science., 2008, 320, 634.

[12] W.S. Liu, Q. Y. Zhang, Y. C Lan, S. Chen, X. Yan, Q. Z., H. Wang, D.Z Wang, G. Chen, and Z. F. Ren, Adv. Energy Mater., 2011, 1, 577.

[13] J. J. Shen, T. J. Zhu, X. B. Zhao, S. N. Zhang, S. H. Yang and Z. Z. Yin, Energy Environ. Sci., 2010, 3, 1519.

[14] G. Joshi, H. Lee, Y. C. Lan, X. W. Wang, G. H. Zhu, D. Z Wang, R. W. Gould, D. C. Cuff, M. Y. Tang, M. S. Dresselhaus, G. Chen, and Z. F. Ren, Nano Lett., 2008, 8, 4670.

[15] K. Favier, G. B.Granger, C. Navone, M. Soulier, M. Boidot, J. Leforestier, J. Simon, J. C Tedenac, D. Ravot, Acta Mater., 2014, 64, 429.

[16] M. Zhou, J. F. Li, and T. Kita, J. Am. Chem. Soc., 2008, 130, 4527.

[17] K. F. Hsu, S. Loo, F. Guo, W. Chen, J. S. Dyck, C. Uher, T. Hogan, E. K. Polychroniadis and M. G. Kanatzidis, Science., 2004, 303, 818.

[18] R. AMATYA and R. J. RAM, J. Electron. Mater., 2012, 41, 1011.

[19] G. Tan, W. Liu, H. Chi, X. Su, S. Wang, Y. Yan, X. Tang, W. Wong-Ng and C. Uher, Acta Mater., 2013, 61, 7693.

[20] X. Shi, J. Yang, J. R. Salvador, M. Chi, J. Y. Cho, H. Wang, S. Bai, J. Yang, W. Zhang and L. Chen, J. Am. Chem. Soc., 2011, 133, 7837.

[21] S. Chen and Z. F. Ren, Materials Today., 2013, 16, 387.

[22] L. D. Zhao, S. Q Hao, S. H. Lo, C. I Wu, X. Y. Zhou, Y Lee, H. Li, K. Biswas, T. P. Hogan, C. Uher, C. Wolverton, V. P. Dravid, and M. G. Kanatzidis, J. Am. Chem. Soc., 2013, 135, 7364.

[23] L. D. Zhao, S. H. Lo, J. Q. He, H. Li, K. Biswas, J. Androulakis, C. I Wu, T. P. Hogan, D.Y. Chung, V. P. Dravid and M. G. Kanatzidis, J. Am. Chem. Soc., 2011, 133, 20476.

[24] W. Liu, X. J. Tan, K. Yin, H. J. Liu, X. F. Tang, J. Shi, Q. J. Zhang and C. Uher, Phys. Rev. Lett., 2012, 108, 166601.

[25] A.U. Khan, N. Vlachos, Th. Kyratsi, Scri Mater., 2013, 69, 606.

[26] J. S. Rhyee, K. H. Lee, S. M. Lee, E. Cho, S. Il Kim, E. Lee, Y. S. Kwon, J. H. Shim and G. Kotliar, Nature., 2009, 459, 965.

[27] S. N. Guin, A. Chatterjee, D. S. Negi, R. Datta and K. Biswas, Energy Environ.

Sci., 2013, 6, 2603.

[28] S. N. Guin, D. S. Negi, R. Datta and K. Biswas, J. Mater. Chem. A., 2014, 2, 4324.

[29] S. N. Guin, A. Chatterjee and K. Biswas, RSC Adv., 2014, 4, 11811.

[30] Q. Zhang, F. Cao, W. S. Liu, K. Lukas, B. Yu, S. Chen, C. Opeil, D. Broido, G. Chen, and Z. F. Ren, J. Am. Chem. Soc., 2012, 134, 10031.

[31] H. Z. Zhao, J. H. S, Z. J. Tang, Y. C. Lan, Q. Jie, D. Kraemer, K. McEnaney, A. Guloy, G. Chen, Z. F. Ren, Nano Energy., 2014, 7, 97.

[32] E Botcharovaa, M Heilmaiera, J Freudenbergera, G Drewa, D Kudashowb,U Martinb, L Schultza, J. Alloys Comp., 2003, 351, 119.

[33] J. P. Heremans, C. M. Thrush and D. T. Morelli, Phys. Rev. B., 2004, 70, 115334.

[34] C. L. Wan, Y. F. Wang, W. Norimatsu, M. Kusunoki and K. Koumoto, Appl. Phys. Lett., 2012, 100, 10193.

Figure and Table captions

Figure 1. (a) Power XRD patterns, (b) Partly enlarged XRD patterns; (c) Corresponding lattice parameter of $AgNa_xSb_{1-x}Se_2$ of $AgNa_xSb_{1-x}Se_2$（x=0, 0.005, 0.01, 0.02）samples;.

Figure 2. SEM and elemental distribution of $AgNa_{0.01}Sb_{0.99}Se_2$. (a) Low magnification (b) Medium magnification SEM image of fracture morphology of the

$AgNa_{0.01}Sb_{0.99}Se_2$ sample, inset shows the image of microprecipitates; (c–f) Elemental distribution of Ag, Sb, Se and Na obtained from EDX.

Figure 3. High-magnification TEM image with inset FFT image of pristine $AgSbSe_2$ (a) and $AgNa_{0.01}Sb_{0.99}Se_2$ (b).

Figure 4. Temperature dependent thermoelectric properties for $AgNa_xSb_{1-x}Se_2$（x=0, 0.005, 0.01, 0.02）(a) electrical conductivity;(b) Seebeck coefficient; (c) Power factor; (d) Thermal conductivity; (e) Lattice thermal conductivity and (f) Figure of merit, ZT

Table 1. carrier concentrations and mobilities of $AgNa_xSb_{1-x}Se_2$ (x=0、0.005、0.01、0.02) at room temperature

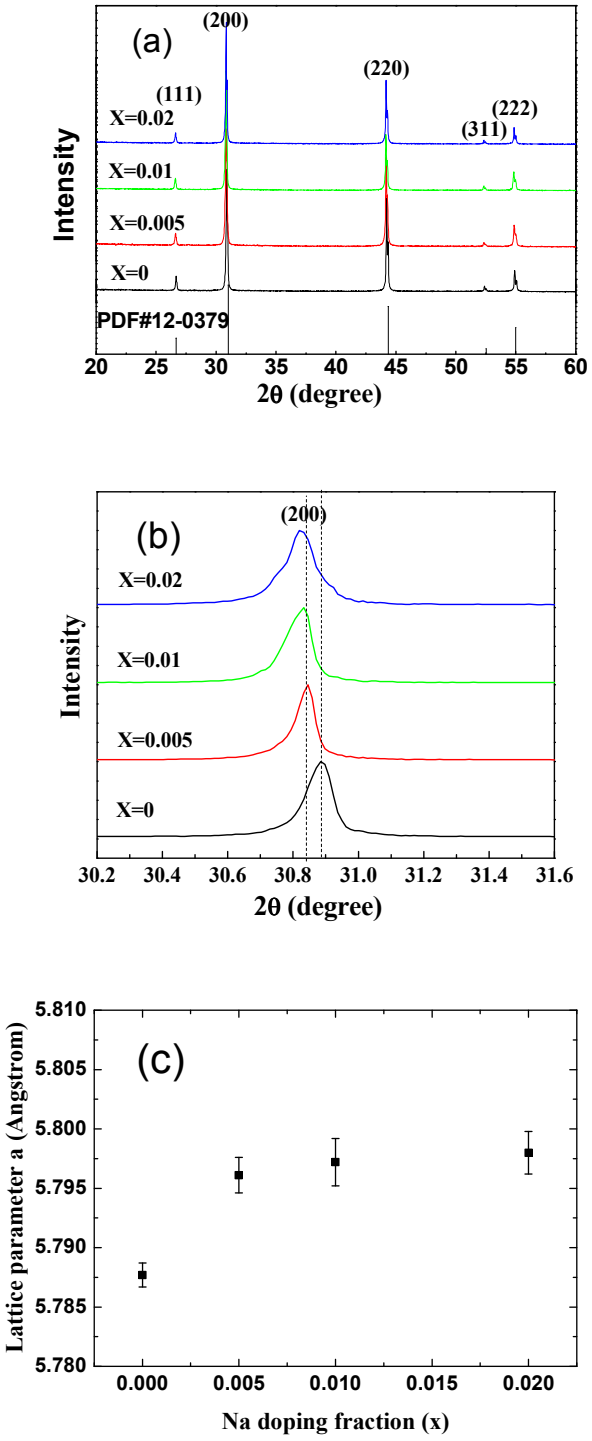

Figure 1

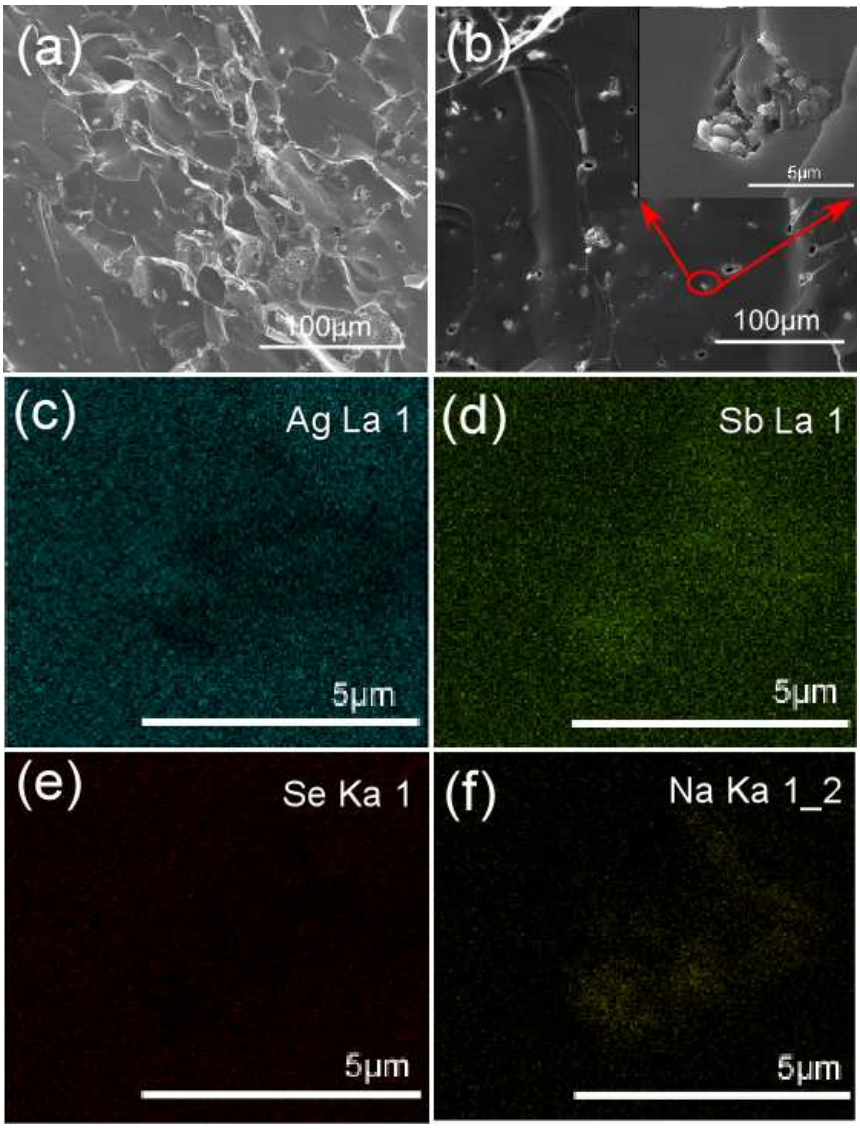

Figure 2

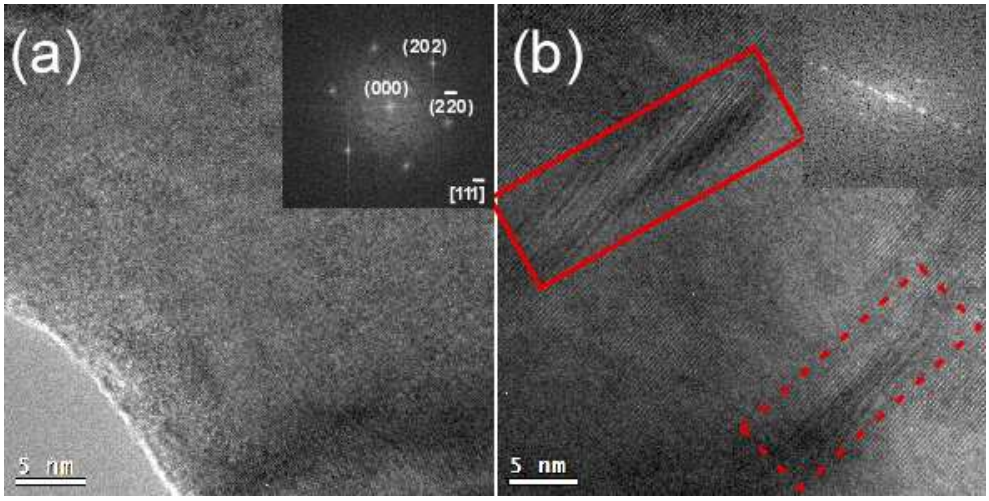

Figure 3

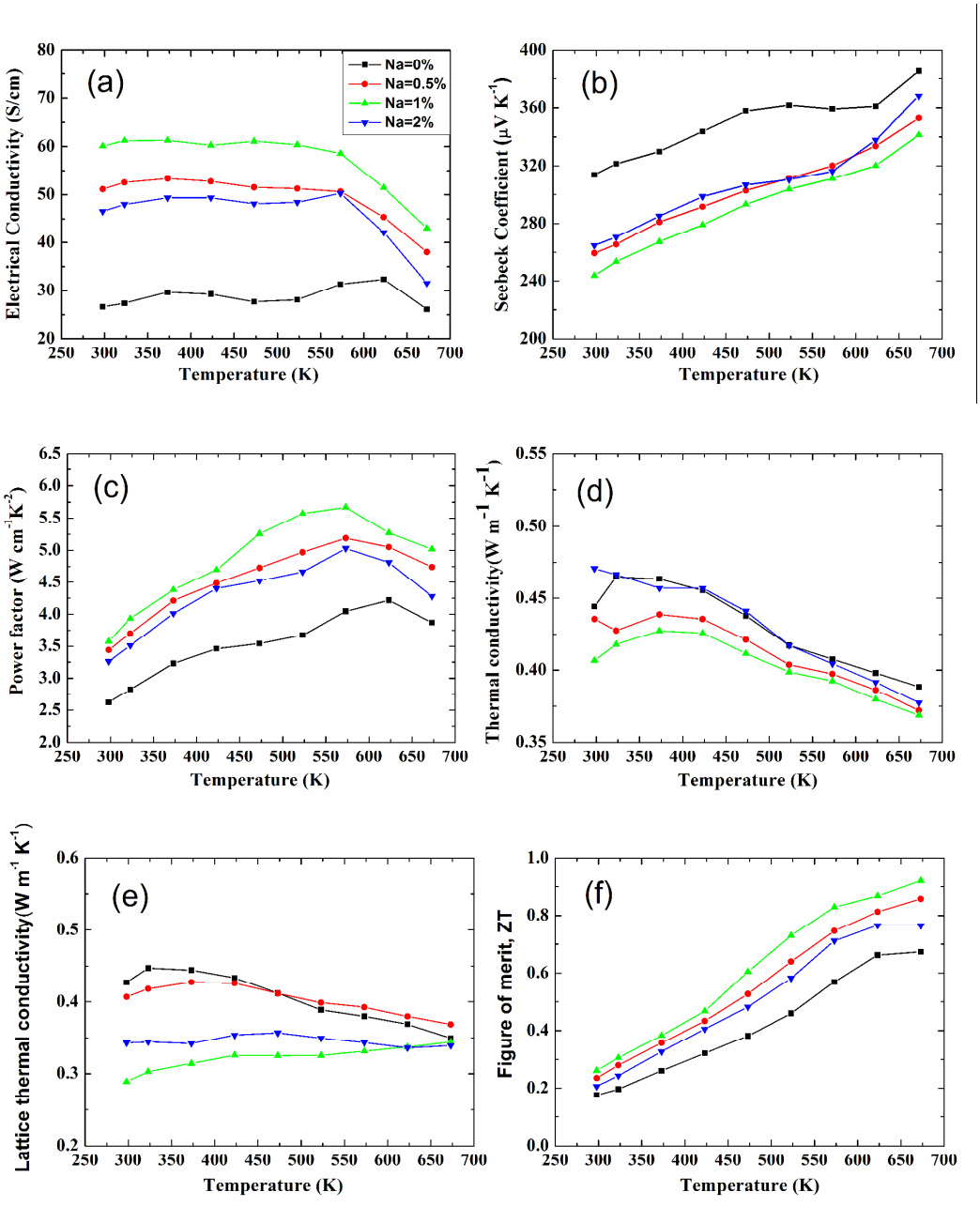

Figure 4

Table 1

Composition	Carrier concentration (10^{19} cm^{-3})	Mobility (cm^2 $V^{-1}S^{-1}$)
$AgSbSe_2$	0.77	29.1
$AgNa_{0.005}Sb_{0.995}Se_2$	3.1	10.3
$AgNa_{0.01}Sb_{0.99}Se_2$	3.9	9.6
$AgNa_{0.02}Sb_{0.98}Se_2$	4.2	6.6